Available online at www.sciencedirect.com
SCIENCE DIRECT®
Journal of Power Sources 142 (2005) 160–168
JOURNAL OF POWER SOURCES
www.elsevier.com/locate/jpowsour

# A methodology for thermodynamic simulation of high temperature, internal reforming fuel cell systems

José Alexandre Matelli*, Edson Bazzo[1]

*Federal University of Santa Catarina, Mechanical Engineering Department, Laboratory of Combustion and Thermal System Engineering, Campus Universitário, Trindade, 88040-900 Florianópolis, SC, Brazil*

Received 31 August 2004; accepted 29 September 2004
Available online 22 December 2004

**Abstract**

This work presents a methodology for simulation of fuel cells to be used in power production in small on-site power/cogeneration plants that use natural gas as fuel. The methodology contemplates thermodynamics and electrochemical aspects related to molten carbonate and solid oxide fuel cells (MCFC and SOFC, respectively). Internal steam reforming of the natural gas hydrocarbons is considered for hydrogen production. From inputs as cell potential, cell power, number of cell in the stack, ancillary systems power consumption, reformed natural gas composition and hydrogen utilization factor, the simulation gives the natural gas consumption, anode and cathode stream gases temperature and composition, and thermodynamic, electrochemical and practical efficiencies. Both energetic and exergetic methods are considered for performance analysis. The results obtained from natural gas reforming thermodynamics simulation show that the hydrogen production is maximum around 700 °C, for a steam/carbon ratio equal to 3. As shown in the literature, the found results indicate that the SOFC is more efficient than MCFC.


*Keywords:* Fuel cell; Simulation; Natural gas reforming; Hydrogen

## 1. Introduction

In the current worldwide energy scenario, fuel cells are presented as an emergent technology for power production. They are devices that convert the chemical energy of a fuel directly to power through an electrochemical process that has no relation with the Carnot's cycle and its efficiency. Thus, the efficiency of a fuel cell is comparatively higher than the efficiency of a conventional thermodynamic cycle (the Rankine cycle, for instance) and reaches values as high as 45%. Depending on their characteristics, fuel cells can be used either in small on-site power/cogeneration plants or as a power sources for vehicles. In most cases, the fuel cell uses hydrogen as fuel and oxygen as oxidizing agent.

The major advantages of fuel cells are high efficiency, low on-site emissions, clean and quiet operation, modularity and fast load response. On the other hand, the costs are very high and obtaining the hydrogen is not a trivial task. Despite the disadvantages, fuel cells are considered a promising alternative to power production within a sustainable and clean energy production context.

This work presents a methodology for fuel cells thermodynamic simulation. Two types of fuel cells are analysed: molten carbonate fuel cell (MCFC) and solid oxide fuel cell (SOFC). Their high operation temperature, 650 and 900 °C, respectively, characterizes these kinds of cells. Internal steam reforming of natural gas, that is, the reforming reaction occurring inside the fuel cell anode, is considered in hydrogen production. The fuel cells are simulated in order to evaluate and compare their respective energetic, exergetic and

* Corresponding author. Tel.: +55 48 331 9390; fax: +55 48 331 7615.
*E-mail addresses:* matelli@cet.ufsc.br (J.A. Matelli), ebazzo@emc.ufsc.br (E. Bazzo).
[1] Tel.: +55 48 331 9812; fax: +55 48 331 7615.

0378-7753/$ – see front matter © 2004 Elsevier B.V. All rights reserved.
doi:10.1016/j.jpowsour.2004.09.039

**Nomenclature**

| | |
|---|---|
| $a, b, c, \ldots$ | number of moles of a specie in a chemical reaction |
| $\overline{c}_p$ | specific heat (kJ kmol$^{-1}$ K$^{-1}$) |
| $\overline{e}$ | specific exergy (kJ kmol$^{-1}$) |
| $\dot{E}x$ | exergy transfer rate (kW) |
| $F$ | Faraday's constant (9.64867 × 107 C kmol$^{-1}$) |
| $G$ | Gibbs' free energy (kJ) |
| $\overline{h}$ | specific enthalpy (kJ kmol$^{-1}$) |
| $H$ | enthalpy (kJ) |
| $\dot{I}$ | irreversibility transfer rate (kW) |
| LHV | lower heating value (kJ kg$^{-1}$) |
| $\dot{m}$ | mass flow (kg s$^{-1}$) |
| $\dot{n}$ | molar flow (kmol s$^{-1}$) |
| $N$ | number of cells in a stack; mole number |
| $P$ | pressure (kPa) |
| $Q$ | heat (kJ) |
| $\dot{Q}$ | heat transfer rate (kW) |
| $\overline{R}$ | universal gases constant (8.31434 kJ kmol$^{-1}$ K$^{-1}$) |
| $\overline{s}$ | specific entropy (kJ kmol$^{-1}$ K$^{-1}$) |
| $S$ | entropy (kJ K$^{-1}$) |
| $T$ | absolute temperature (K) |
| $U$ | internal energy (kJ) |
| $V$ | volume (m$^3$); electrode potential (V) |
| $W$ | work (kJ) |
| $\dot{W}$ | power output; work transfer rate (kW) |
| $X$ | molar fraction |

*Greeks*

| | |
|---|---|
| $\varepsilon$ | cell voltage (V) |
| $\eta$ | efficiency (%) |
| $\lambda$ | steam–carbon rate |
| $\xi$ | standard chemical exergy (kJ kmol$^{-1}$) |
| $\phi$ | hydrogen utilization factor |
| $\psi$ | rational efficiency (%) |

*Subscripts*

| | |
|---|---|
| an | anode |
| anc | ancillary |
| cel | cell |
| ch | chemical |
| ct | cathode |
| el | electric |
| elq | electrochemical |
| eq | equilibrium |
| g | gas |
| in | inlet |
| I | first law of thermodynamics |
| II | second law of thermodynamics |
| $j$ | $j$th specie |
| l | liquid |
| net | net power |
| ng | natural gas |
| out | outlet |
| ph | physical |
| prt | practical |
| ref | reforming |
| stk | stack |
| th | thermodynamic |

*Superscripts*

| | |
|---|---|
| 0 | reference state (101.3 kPa and 298.15 K) |
| $Q$ | heat |

environmental performances, based on the amount of $CO_2$ emissions.

## 2. Fuel cell system description

The fuel cells considered in this work are MCFC and SOFC, to be used in a 900 $kW_{el}$ natural gas on-site power plant, as one can seen in Figs. 1 and 2. Both fuel cells operate with internal reforming of natural gas.

In the MCFC system illustrated in Fig. 1, natural gas (point 1) and water (point 9) are admitted into the double heat exchanger to pre-heat the gas stream and to generate steam. The pre-heated natural gas (point 2) and the steam (point 10) flow

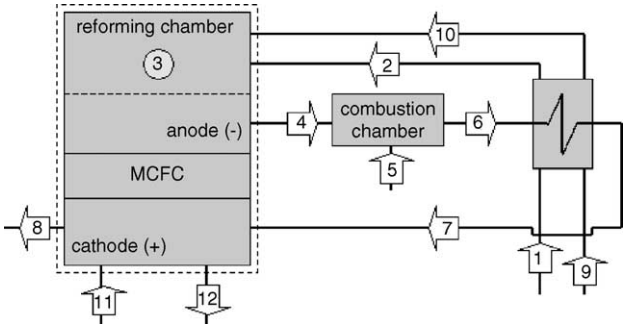


Fig. 1. MCFC fuel cell system.

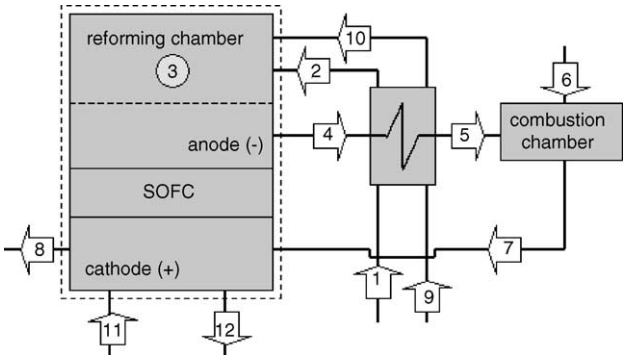


Fig. 2. SOFC fuel cell system.

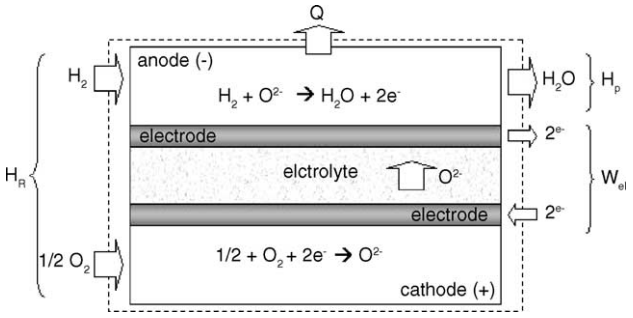


Fig. 3. System for fuel cell analysis.

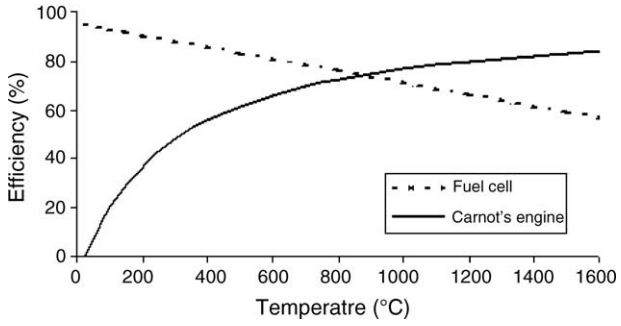


Fig. 4. Comparison between the efficiencies of a fuel cell and a Carnot's engine [1].

to the reforming chamber in the anode side of the fuel cell (point 3), where the steam reforming reaction occurs while the hydrogen produced in the reforming is consumed in the electrochemical reaction. The heat associated to the combustion of the synthesis gas leaving the anode (point 4) in the combustion chamber (with additional air from point 5) is recovered in the heat exchanger. The system is adjusted such that the energy associated to the exhaust gases leaving the combustion chamber (point 6) is exactly sufficient for gas pre-heating and steam production. The required temperature is guaranteed by the amount of air (point 5) supplied to the combustion reaction. The oxygen contained in the exhaust gases from the combustion chamber (point 7) is used in the cathode to complete the electrochemical reaction, and the resulting exhaust gases are rejected to the ambient. Water is also used in the cathode cooling system (points 11 and 12).

The SOFC system illustrated in Fig. 2 is similar to the MCFC system, except that in the SOFC system the heat exchanger is placed between the anode and combustion chamber.

## 3. Theoretical analysis of the fuel cell system

### 3.1. Thermodynamic analysis

Fuel cell is a device that converts the Gibbs' free energy of a fuel directly into power. This statement is demonstrated here based on the work from Kordesch and Simader [1] for $H_2$–$O_2$ fuel cells, as shown in Fig. 3, considering the chemical reaction (Eq. (1)):

$$H_{2(g)} + \tfrac{1}{2}O_{2(g)} \rightarrow H_2O_{(l)} \tag{1}$$

Applying the first law of thermodynamics, neglecting kinetic and potential energy variations:

$$\delta Q - \delta W = \mathrm{d}U \tag{2}$$

But,

$$\mathrm{d}U = \mathrm{d}H - P\mathrm{d}V - V\mathrm{d}P \tag{3}$$

Considering isobaric process and introducing Eq. (3) into Eq. (2), we have

$$\delta Q - \delta W = \mathrm{d}H - P\mathrm{d}V \tag{4}$$

Since in a fuel cell, the reactions are electrochemical, the work in Eq. (4) is related to the work for the expansion of the gases plus the work due to the transport of electrical charges through the external circuit connecting the anode to the cathode. Thus,

$$\delta W = \delta W_{\mathrm{el}} + P\mathrm{d}V \tag{5}$$

If the process is considered reversible, the second law results in

$$\delta Q = T\mathrm{d}S \tag{6}$$

The electrical work is obtained substituting Eqs. (5) and (6) into Eq. (4) and rewriting, obtaining

$$\delta W_{\mathrm{el}} = T\mathrm{d}S - \mathrm{d}H = -\mathrm{d}G \tag{7}$$

As stated before, Eq. (7) shows that the maximum work is the Gibbs' free energy obtained from the cell global reaction (Eq. (1)). Considering products and reactants at reference state ($T$ = 298.15 K, $P$ = 101.3 kPa) and integrating, we have

$$W_{\mathrm{el}}^0 = -\Delta G^0 \tag{8}$$

The thermodynamic efficiency of a fuel cell is defined as the maximum work obtained in the cell divided by the energy released in the reversible isobaric global chemical reaction, as shown by Eq. (9):

$$\eta_{\mathrm{th}} = \frac{\Delta G}{\Delta H} = 1 - \frac{T\Delta S}{\Delta H} \tag{9}$$

Therefore, it is clear that the thermodynamic efficiency of a fuel cell has no relation with the Carnot's cycle efficiency, because a fuel cell is an electrochemical device while a Carnot's engine is a thermal machine that operates between two heat reservoirs. A comparison between the efficiencies of a fuel cell and of a Carnot's engine is showed in Fig. 4.

### 3.2. Electrochemical analysis

The fuel cell electrical work (or its power output) can be written as a function of the difference of potential between

the electrodes, as expressed in Eq. (10):

$$W_{el} = nF(V_{ct} - V_{an}) = nF\varepsilon_{cel} \quad (10)$$

Replacing Eqs. (10) into (7), we have

$$\Delta G^0 = -nF\varepsilon^0_{cel} \quad (11)$$

In the case of a $H_2$–$O_2$ fuel cell (see Fig. 3), the balance of charges requires that

$$n = 2n_{H_2} \quad (12)$$

From Eq. (11), it follows that $\varepsilon^0_{cel}$ is the cell reversible potential, that is, the maximum possible difference of potential between the fuel cell electrodes. Since, it is not possible to measure the potential of an isolated electrode, by convention the hydrogen electrode is adopted as the reference electrode, whose potential is set to zero. The potential values for several electrochemical reactions are listed in [2]. Thus, for a fuel cell based in Eq. (1), the reversible potential is 1.229 V. However, several phenomena related to the kinetics of the electrochemical conversion in the electrodes introduce losses in the cell potential as the current intensity increases, as shown in Fig. 5. These losses are known as overpotential or overvoltage and their origin are not discussed in this work.

The overpotential effects can be quantified through the *electrochemical efficiency*, defined as the real voltage of a cell divided by its maximum voltage, as showed by Eq. (13):

$$\eta_{elq} = \frac{\varepsilon_{cel}}{\varepsilon^0_{cel}} = \frac{W_{el}}{W^0_{el}} \quad (13)$$

Eq. (13) can also be used to measure the quality of a fuel cell. Different technical projects of fuel cells, operating with the same reaction and with the same enthalpy, may present different electrochemical efficiency. Values as high as 90% for the electrochemical efficiency can be reached in $H_2$–$O_2$ fuel cells [1]. Since the power output of a cell is equal to the voltage times its current, the maximum cell electrochemical efficiency—and also the *maximum cell thermodynamic efficiency*—occurs when the power output is zero, because $\varepsilon_{cel} = \varepsilon^0_{cel}$ when the current is zero, as one can seen from Fig. 5.

The *practical efficiency* is defined as the real cell power output divided by the fuel enthalpy (see Eq. (26)), or as the thermodynamic efficiency multiplied by the electrochemical efficiency:

$$\eta_{prt} = \frac{W_{el}}{\Delta H} = \frac{nF\varepsilon_{cel}}{\Delta H} = \eta_{th}\eta_{elq} \quad (14)$$

For a fuel cell operating with hydrogen from natural gas reforming, the overall efficiency is associated to the total power output and the natural gas lower heating value. In this work, this efficiency is named first law efficiency, and is given by

$$\eta_I = \frac{\dot{W}_{el}}{\dot{m}_{ng}\mathrm{LHV}_{ng}} \quad (15)$$

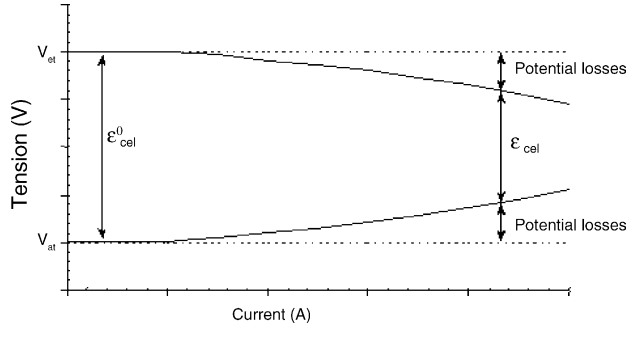


Fig. 5. Potential losses in a fuel cell.

### 3.3. Thermochemical aspects: natural gas reforming

Since hydrogen is available in its free form (as $H_2$ gas), it must be obtained from other molecules. Among several methods of hydrogen generation, the hydrocarbon reforming has been the most used, especially methane reforming, due to its abundance in natural gas compositions. Furthermore, the hydrogen concentration in the resulting stream gases is relatively high. The stream gas resulting from the reforming is named generically synthesis gas and its composition is typically $H_2$, CO, $CO_2$, $H_2O$ and traces of other minor species. The exact composition depends on reforming type, temperature and pressure of reaction, steam/carbon ratio and catalyst. Among the methane reforming methods, the major three processes are the autothermal reforming, partial oxidation and steam reforming [3]. The last one is considered in this work, whose global reforming reaction can be represented as

$$CH_4 + aH_2O \rightarrow bCO + cCO_2 + dH_2 + eH_2O \quad (16)$$

Steam reforming is a strongly endothermic reaction. Steam reacts with methane to produce CO, $CO_2$ and $H_2$. This process produces relatively high $H_2$ concentration (usually higher than 50%).

## 4. Performance analysis procedure

To determine the performance parameters, the energy and exergy balances are considered for a fuel cell system. Initially, the natural gas consumption or, specifically, the hydrogen from natural gas steam reforming consumption must be calculated. The hydrogen amount supplied to the anode depends on the equilibrium composition of the reforming reaction (Eq. (17)), which is a function of temperature, pressure and steam/carbon ratio, defined as the mole number of steam divided by the mole number of carbon in the fuel. Generically, we can represent as

$$X_{H_2,eq} = f(T, P, \lambda) \quad (17)$$

The method of element potentials (MEP) is used to find the equilibrium composition of reforming reaction. Using the Lagrange multipliers, the MEP finds the equilibrium point where the Gibbs' free energy of the system is minimized,

Table 1
Typical natural gas composition [5]

| Component | Volumetric fraction (%) | Mass fraction (%) |
|---|---|---|
| $CH_4$ | 90 | 82.2 |
| $C_2H_6$ | 6 | 10.3 |
| $N_2$ | 3 | 4.8 |
| $CO_2$ | 1 | 2.7 |

subject to the atomic population of the reactants. In this work, the MEP is used to simulate the natural gas steam reforming process, using the STANJAN Chemical Equilibrium Solver [4]. It is considered that $P = 101.3$ kPa, $\lambda = 3$ and a typical natural gas composition as presented in Table 1.

With the equilibrium composition of natural gas steam reforming, it is possible to simulate the fuel cells. The MCFC and SOFC electrochemical reactions are described below.

MCFC:

- anode:

$$H_2 + CO_3^{2-} \rightarrow H_2O + CO_2 + 2e^-$$

- cathode:

$$CO_2 + \tfrac{1}{2}O_2 + 2e^- \rightarrow CO_3^{2-}$$

- global:

$$H_2 + \tfrac{1}{2}O_2 \rightarrow H_2O$$

SOFC:

- anode:

$$H_2 + O_2^- \rightarrow H_2O + 2e^-$$

- cathode:

$$\tfrac{1}{2}O_2 + 2e^- \rightarrow O^{2-}$$

- global:

$$H_2 + \tfrac{1}{2}O_2 \rightarrow H_2O$$

Both MCFC and SOFC operate at temperatures high enough to perform the steam reforming inside the anode. This process is known as *internal reforming*. The first step of the cell simulation is to determine the size of the stack, that is, how many cells must be serially connected to achieve the desired voltage

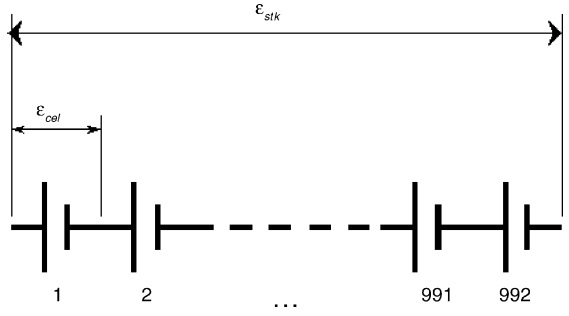


Fig. 6. Scheme of a stack containing 992 cells.

Table 2
$\varepsilon$ and $\phi$ for each type of cell

| Cell | $\varepsilon$ (V) | $\phi$ |
|---|---|---|
| IRMCFC | 0.6663 | 0.90 |
| IRSOFC | 0.6704 | 0.95 |

and, consequently, the desired power output. In this work, we consider 992 cells for each stack, as suggested in Fig. 6. This value is obtained from a 200 $kW_{el}$ commercially available phosphoric acid fuel cell. From cell voltage and power, the hydrogen consumption of electrochemical reaction is given by Eq. (18), re-written from Eq. (11):

$$\dot{n}_{H_2,cel} = \frac{\dot{W}_{cel}}{2F\varepsilon_{cel}} \tag{18}$$

The hydrogen consumption of each cell is a function of the hydrogen utilization factor, $\phi$, defined as the ratio between the hydrogen amount which is consumed in the electrochemical reaction and the total amount of hydrogen which is supplied to the anode, as one can seen in Eq. (19):

$$\phi = \frac{\dot{n}_{H_2,cel}}{\dot{n}_{H_2,an}} \tag{19}$$

The voltage of each type of cell is showed in Table 2, which values are found in the literature and also stated by manufacturers of functional prototypes. Since the voltage values presented in Table 2 are lower than 1.229 V, it is clear that the overpotential effects are taken into account. The hydrogen utilization factor is also presented in this table.

The stack hydrogen consumption is written as the sum of the consumption of each individual cell:

$$\dot{n}_{H_2,stk} = N\dot{n}_{H_2,an} \tag{20}$$

The natural gas consumption of the stack is related to the hydrogen consumption through the steam reforming equilibrium composition, defined in Eq. (17):

$$\dot{n}_{ng,stk} = \frac{\dot{n}_{H_2,stk}}{X_{H_2,eq}} \tag{21}$$

In order to perform the energy balance in the stack (Fig. 7), it is necessary to know the enthalpies and entropies at the inlet and outlet stream gases. In this work, the stream gases are

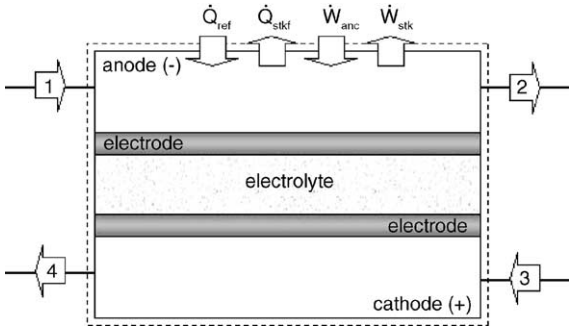


Fig. 7. Energy balance.

considered as perfect gases, which enthalpies and entropies are calculated according Eqs. (22) and (23). In Eq. (23), the logarithm term is not considered, because it is very small when compared to other terms. The heat rejected is calculated from an energy balance, according to Eq. (24). A significant amount of the heat generated by the stack is absorbed by the reforming reaction. The several auxiliary control systems of the stack consume a part of the power produced:

$$\bar{h} = \sum_{j=1}^{n} X_j \left( \bar{h}_j^0 + \int_{T_0}^{T} \bar{c}_{p_j} \mathrm{d}T \right) \tag{22}$$

$$\bar{s} = \sum_{j=1}^{n} X_j \left( \bar{s}_j^0 + \int_{T_0}^{T} \left( \frac{\bar{c}_{p_j}}{T} \right) \mathrm{d}T - \bar{R} \ln X_j \right) \tag{23}$$

$$\dot{Q}_{\mathrm{ref}} - \dot{Q}_{\mathrm{stk}} + \dot{W}_{\mathrm{stk}} - \dot{W}_{\mathrm{aux}} = \sum \dot{n}_{\mathrm{out}} \bar{h}_{\mathrm{out}} - \sum \dot{n}_{\mathrm{in}} \bar{h}_{\mathrm{in}} \tag{24}$$

The thermodynamic, electrochemical and practical efficiencies are calculated from the Gibbs' free energy, according to the following equations:

$$\Delta H_{\mathrm{stk}} = \dot{n}_{\mathrm{H_2O,stk}} \bar{h}_{\mathrm{H_2O}} - \dot{n}_{\mathrm{O_2,stk}} \bar{h}_{\mathrm{O_2}} - \dot{n}_{\mathrm{H_2,stk}} \bar{h}_{\mathrm{H_2}} \tag{25}$$

$$\Delta S_{\mathrm{stk}} = \dot{n}_{\mathrm{H_2O,stk}} \bar{s}_{\mathrm{H_2O}} - \dot{n}_{\mathrm{O_2,stk}} \bar{s}_{\mathrm{O_2}} - \dot{n}_{\mathrm{H_2,stk}} \bar{s}_{\mathrm{H_2}} \tag{26}$$

$$\Delta G_{\mathrm{stk}} = \Delta H_{\mathrm{stk}} - T_{\mathrm{cel}} \Delta S \tag{27}$$

To complete the simulation, the energy, mass and exergy balances are performed in the combustion chamber and in the heat exchanger, according to

$$\dot{Q} - \dot{W} = \sum \dot{n}_{\mathrm{out}} \bar{h}_{\mathrm{out}} - \sum \dot{n}_{\mathrm{in}} \bar{h}_{\mathrm{in}} \tag{28}$$

$$\sum \dot{m}_{\mathrm{in}} = \sum \dot{m}_{\mathrm{out}} \tag{29}$$

$$\dot{E}x^{\dot{Q}} - \dot{W} - \dot{I} = \sum \dot{n}_{\mathrm{out}} \bar{e}_{\mathrm{out}} - \sum \dot{n}_{\mathrm{in}} \bar{e}_{\mathrm{in}} \tag{30}$$

In Eq. (30), the exergies are calculated according to the following equations:

$$\dot{E}x^{\dot{Q}} = \dot{Q} \left[ \frac{T - T_0}{T} \right] \tag{31}$$

$$\bar{e} = \bar{e}_{\mathrm{ph}} + \bar{e}_{\mathrm{ch}} \tag{32}$$

$$\bar{e}_{\mathrm{ph}} = (\bar{h} - \bar{h}_0) - T_0(\bar{s} - \bar{s}_0) \tag{33}$$

$$\bar{e}_{\mathrm{ch}} = \sum_{j=1}^{N} X_j \xi_j + T_0 \bar{R} (X_j \ \ln \ X_j) \tag{34}$$

In Eq. (34), $\xi_j$ is the standard chemical exergy of the $j$th specie. In Table 3 are presented the values of $\xi$ of the chemical species considered in this work.

The exergy balance leads to the concept of rational efficiency, defined as the ratio between the total outlet exergy and the total inlet exergy, according to Eq. (35):

$$\psi = \frac{\Delta \dot{E}x_{\mathrm{out}}}{\Delta \dot{E}x_{\mathrm{in}}} = 1 - \frac{\dot{I}}{\Delta \dot{E}x_{\mathrm{in}}} \tag{35}$$

The second law efficiency of a system is defined as the ratio between the useful power output and the natural gas exergy, according to Eq. (36). The natural gas exergy is calculated from Eq. (34):

$$\eta_{\mathrm{II}} = \frac{\dot{W}_{\mathrm{net}}}{\dot{E}x_{\mathrm{ng}}} \tag{36}$$

Finally, the $CO_2$ emission is calculated based on the natural gas reforming reaction and natural combustion reaction (Eq. (37)):

$$a\mathrm{CH_4} + b\mathrm{C_2H_6} + c\mathrm{CO_2} + d\mathrm{N_2} + e(\mathrm{O_2} + 3.76\mathrm{N_2}) \rightarrow f\mathrm{CO_2} + g\mathrm{H_2O} + h\mathrm{O_2} + i\mathrm{N_2} \tag{37}$$

Table 3
Standard chemical exergy [6]

| $j$ | Specie | $\xi$ (kJ kmol$^{-1}$) |
|---|---|---|
| 1 | $H_2$ | 238490 |
| 2 | CO | 275430 |
| 3 | $CO_2$ | 20140 |
| 4 | $H_2O$ | 11710 |
| 5 | $CH_4$ | 836510 |
| 6 | $C_2H_6$ | 1504360 |
| 7 | $N_2$ | 720 |
| 8 | $O_2$ | 3970 |

## 5. Results

The molar fractions found in the reforming reaction simulation are presented in Fig. 8. From this figure, one can see that for the MCFC internal reforming process ($T = 650\,^{\circ}\mathrm{C}$) the hydrogen molar fraction is greater than the SOFC one ($T = 900\,^{\circ}\mathrm{C}$). In fact, the hydrogen production at 650 °C is

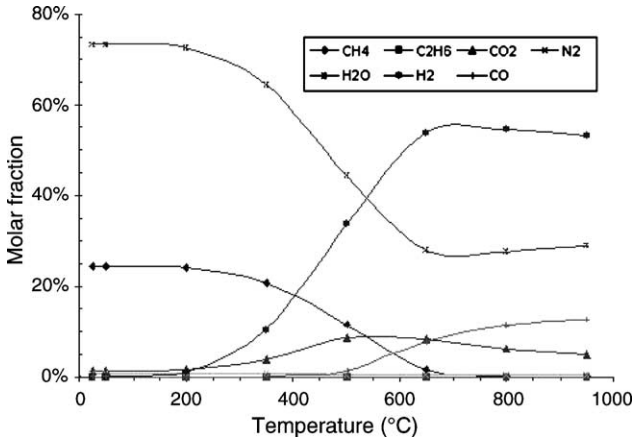


Fig. 8. Molar fraction found for natural gas reforming simulation.

Table 4
Results from fuel cells simulation

| Fuel cell | $T$ (°C) | $\varepsilon_{stk}$ (V) | $i$ (A) | $\dot{W}_{stk}$ (kW) | $\dot{W}_{aux}$ (kW) | $\Delta H$ (kW) | $\Delta S$ (kW K$^{-1}$) | $\Delta G$ (kW) | $\eta_{th}$ (%) | $\eta_{elq}$ (%) | $\eta_{prt}$ (%) | $\eta_{I}$ (%) | $\eta_{II}$ (%) |
|---|---|---|---|---|---|---|---|---|---|---|---|---|---|
| MCFC | 650 | 661 | 1511 | 999 | 99 | −1921 | −0.4254 | −1529 | 79.6 | 65.4 | 52.0 | 40.1 | 37.7 |
| SOFC | 900 | 665 | 1435 | 954 | 54 | −1835 | −0.4145 | −1349 | 73.5 | 70.7 | 52.0 | 46.3 | 43.4 |

Table 5
Rational efficiency of the MCFC and SOFC plant components

| Component | $\dot{E}x_{in}$ (kW) | $\dot{E}x_{out}$ (kW) | $\dot{I}$ (kW) | $\psi$ (%) |
|---|---|---|---|---|
| MCFC | 3608 | 3118 | 490 | 86.4 |
| Heat exchanger | 3352 | 3156 | 196 | 94.2 |
| Combustion chamber | 1327 | 963 | 364 | 72.6 |
| SOFC | 2715 | 2423 | 292 | 89.2 |
| Heat exchanger | 3021 | 2882 | 139 | 95.4 |
| Combustion chamber | 750 | 439 | 311 | 58.5 |

near the maximum. The MCFC internal reforming process presents carbon monoxide molar fraction smaller than the SOFC one. On the other hand, methane and ethane are completely consumed in the SOFC internal reforming process.

The results obtained from the fuel cells simulations are showed in Table 4. The MCFC presented thermodynamic efficiency greater than the SOFC, because its operation temperature is smaller. This result is in accordance with the theoretical result presented in Fig. 4. In contrast, the SOFC has an electrochemical efficiency greater than the MCFC, because its voltage is greater, resulting in a smaller current for the same power output. Consequently, the overvoltage effects are smaller (see Fig. 3). The practical efficiency was found equal for both cell types. The SOFC has the first and second law efficiencies greater than the MCFC, because its higher operation temperature allows a higher heat recovery in the reforming reaction, resulting in more hydrogen produced, despite its smaller hydrogen molar fraction from the reforming reaction.

In Table 5 are presented the results related to the rational efficiency for each plant component. The SOFC has a greater rational efficiency than MCFC, because the temperatures and chemical species involved in its operation result in a smaller entropy generation. It is interesting to note that the rational efficiency values for both fuel cells are relatively high. In other words, fuel cells are devices that generate power with low entropy generation, that is, close to a reversible cycle. It means that fuel cells have a huge potential for energy saving when compared to those power production technologies

Table 6
MCFC system (see Fig. 1)

| Point | $\dot{m}$ (kg s$^{-1}$) | $\dot{n}$ (kmol s$^{-1}$) | MM (kg kmol$^{-1}$) | $T$ (°C) | $\bar{h}$ (kJ kmol$^{-1}$) | $\bar{s}$ (kJ kmol$^{-1}$ K$^{-1}$) | $\bar{e}_{ph}$ (kJ kmol$^{-1}$) | $\bar{e}_{ch}$ (kJ kmol$^{-1}$) | $\bar{e}$ (kJ kmol$^{-1}$) |
|---|---|---|---|---|---|---|---|---|---|
| 1 | 0.04771 | 0.00272 | 17.52 | 25 | −76398 | 189.3 | 0 | 842315 | 842315 |
| 2 | 0.04771 | 0.00272 | 17.52 | 100 | −73512 | 197.9 | 316 | 842315 | 842631 |
| 3 | 0.1948 | 0.01591 | 12.25 | 650 | −87853 | 197 | 9725 | 166910 | 176636 |
| 4 | 0.6611 | 0.02368 | 27.92 | 650 | −256419 | 240.8 | 11869 | 43699 | 55568 |
| 5 | 0.7279 | 0.02523 | 28.85 | 25 | 0 | 194.3 | 0 | 429.5 | 429.5 |
| 6 | 1.389 | 0.04804 | 28.91 | 801 | −126385 | 242.6 | 14804 | 5238 | 20042 |
| 7 | 1.389 | 0.04804 | 28.91 | 599 | −134423 | 234.3 | 9235 | 5238 | 14473 |
| 8 | 0.9290 | 0.03639 | 25.53 | 576 | −101905 | 227 | 8166 | 4063 | 12229 |
| 9 | 0.1471 | 0.00817 | 18.02 | 25 | 1889 | 6.61 | 0 | 11710 | 11710 |
| 10 | 0.1471 | 0.00817 | 18.02 | 100 | 48207 | 132.6 | 8752 | 11710 | 20462 |
| 11 | 0.6951 | 0.03858 | 18.02 | 25 | 1889 | 6.61 | 0 | 11710 | 11710 |
| 12 | 0.6951 | 0.03858 | 18.02 | 60 | 4526 | 14.97 | 144 | 11710 | 11854 |

Table 7
MCFC System—molar fractions (see Fig. 1)

| Point | $X_{H_2}$ (%) | $X_{CO}$ (%) | $X_{CO_2}$ (%) | $X_{H_2O}$ (%) | $X_{CH_4}$ (%) | $X_{C_2H_6}$ (%) | $X_{N_2}$ (%) | $X_{O_2}$ (%) |
|---|---|---|---|---|---|---|---|---|
| 1 | 0 | 0 | 1 | 0 | 90 | 6 | 3 | 0 |
| 2 | 0 | 0 | 1 | 0 | 90 | 6 | 3 | 0 |
| 3 | 54.26 | 7.810 | 8.137 | 27.60 | 1.680 | 0 | 0.5130 | 0 |
| 4 | 3.646 | 5.247 | 38.28 | 51.35 | 1.129 | 0 | 0.3447 | 0 |
| 5 | 0 | 0 | 0 | 0 | 0 | 0 | 79 | 21 |
| 6 | 0 | 0 | 22.01 | 28.22 | 0 | 0 | 41.49 | 8.281 |
| 7 | 0 | 0 | 22.01 | 28.22 | 0 | 0 | 41.49 | 8.281 |
| 8 | 0 | 0 | 7.707 | 37.26 | 0 | 0 | 54.78 | 0.256 |
| 9 | 0 | 0 | 0 | 100 | 0 | 0 | 0 | 0 |
| 10 | 0 | 0 | 0 | 100 | 0 | 0 | 0 | 0 |
| 11 | 0 | 0 | 0 | 100 | 0 | 0 | 0 | 0 |
| 12 | 0 | 0 | 0 | 100 | 0 | 0 | 0 | 0 |

Table 8
SOFC system (see Fig. 2)

| Point | $\dot{m}$ (kg s$^{-1}$) | $\dot{n}$ (kmol s$^{-1}$) | MM (kg kmol$^{-1}$) | $T$ (°C) | $\bar{h}$ (kJ kmol$^{-1}$) | $\bar{s}$ (kJ kmol$^{-1}$K$^{-1}$) | $\bar{e}_{ph}$ (kJ kmol$^{-1}$) | $\bar{e}_{ch}$ (kJ kmol$^{-1}$) | $\bar{e}$ (kJ kmol$^{-1}$) |
|---|---|---|---|---|---|---|---|---|---|
| 1 | 0.04139 | 0.00236 | 17.52 | 25 | −76398 | 189.3 | 0 | 842315 | 842315 |
| 2 | 0.04139 | 0.00236 | 17.52 | 100 | −73512 | 197.9 | 316 | 842315 | 842631 |
| 3 | 0.1690 | 0.01426 | 11.85 | 900 | −71498 | 204.1 | 15748 | 164723 | 180471 |
| 4 | 0.2870 | 0.01426 | 20.12 | 900 | −192700 | 239.5 | 17983 | 48489 | 66472 |
| 5 | 0.2870 | 0.01426 | 20.12 | 300 | −216186 | 211.7 | 2768 | 49593 | 52362 |
| 6 | 0.6805 | 0.02359 | 28.85 | 25 | 0 | 194.3 | 0 | 128.4 | 128.4 |
| 7 | 0.9675 | 0.03672 | 26.35 | 609 | −83971 | 229.3 | 8877 | 3078 | 11956 |
| 8 | 0.8476 | 0.03304 | 25.66 | 623 | −94923 | 228.8 | 9256 | 3816 | 13073 |
| 9 | 0.1277 | 0.00709 | 18.02 | 25 | 1889 | 6.61 | 0 | 11710 | 11710 |
| 10 | 0.1277 | 0.00709 | 18.02 | 100 | 48207 | 132.6 | 8752 | 11710 | 20462 |
| 11 | 0.2172 | 0.01205 | 18.02 | 25 | 1889 | 6.61 | 0 | 11710 | 11710 |
| 12 | 0.2172 | 0.01205 | 18.02 | 60 | 4526 | 14.97 | 144 | 11710 | 11854 |

Table 9
SOFC system—molar fractions (see Fig. 2)

| Point | $X_{H_2}$ (%) | $X_{CO}$ (%) | $X_{CO_2}$ (%) | $X_{H_2O}$ (%) | $X_{CH_4}$ (%) | $X_{C_2H_6}$ (%) | $X_{N_2}$ (%) | $X_{O_2}$ (%) |
|---|---|---|---|---|---|---|---|---|
| 1 | 0 | 0 | 1 | 0 | 90 | 6 | 3 | 0 |
| 2 | 0 | 0 | 1 | 0 | 90 | 6 | 3 | 0 |
| 3 | 54.42 | 12.12 | 4.929 | 28.03 | 0.005 | 0 | 0.497 | 0 |
| 4 | 2.721 | 12.12 | 4.929 | 79.73 | 0.005 | 0 | 0.497 | 0 |
| 5 | 2.721 | 12.12 | 4.929 | 79.73 | 0.005 | 0 | 0.497 | 0 |
| 6 | 0 | 0 | 0 | 0 | 0 | 0 | 79 | 21 |
| 7 | 0 | 0 | 6.625 | 32.03 | 0 | 0 | 50.74 | 10.60 |
| 8 | 0 | 0 | 7.364 | 35.61 | 0 | 0 | 56.41 | 0.626 |
| 9 | 0 | 0 | 0 | 100 | 0 | 0 | 0 | 0 |
| 10 | 0 | 0 | 0 | 100 | 0 | 0 | 0 | 0 |
| 11 | 0 | 0 | 0 | 100 | 0 | 0 | 0 | 0 |
| 12 | 0 | 0 | 0 | 100 | 0 | 0 | 0 | 0 |

based on combustion, such as internal combustion engines and gas turbines. This is expected, because a combustion reaction is a strongly irreversible process, due to the high differences of temperature involved and due to the high difference of standard chemical exergies involved. Indeed, among the plant components considered in this work, the combustion chamber is the one that presents the lowest efficiency.

In Tables 6–9 are presented the results of the simulation for each point illustrated in Figs. 4 and 5. For simplicity, the pressure in all points was considered constant and equal to 101.3 kPa. The $CO_2$ emission is equal to 0.1234 kg s$^{-1}$ for MCFC and equal to 0.1071 kg s$^{-1}$ for SOFC.

## 6. Conclusion

The methodology presented in this work is appropriate for performance analysis and to understand the thermodynamic behaviour of fuel cells. The thermochemical aspects related to the natural gas reforming were also taken into account. One of the major advantages of the present methodology is its step-by-step formulation, which makes it very easy to simulate in commercial solvers like the EES [7]. The results obtained from natural gas reforming simulation show that the hydrogen production is a maximum around 700 °C, which is close to the MCFC operation temperature. On the other hand at the SOFC operation temperature, methane and ethane are completely reformed. The fuel cells simulation results indicate that the SOFC is more efficient than MCFC and, consequently, the SOFC $CO_2$ emission is lower than the MCFC one. The results found in this work are in good accordance with well-known parameters of fuel cell efficiency found in the literature.

## Acknowledgements

The authors would like to express their gratitude to Prof. Ivo Martinac, from the Royal Institute of Technology, in Stockholm, Sweden and to the CAPES – Coordination of Enhancement for Brazilian Graduated Professionals.

## References

[1] K. Kordesch, G. Simader, Fuel Cells and their Applications, 1st ed., VCH Verlagsgesellschaft mbH, Weinheim, Federal Republic of Germany, 1996, pp. 23–26, 47.
[2] R.T. DeHoff, Thermodynamics in material science, 1st ed., McGraw-Hill, New York, USA, 1993, p. 472.

[3] S. Ahmed, M. Krumpelt, Int. J. Hydrogen Energy 26 (2001) 291–301.
[4] W.C. Reynolds, STANJAN Chemical Equilibrium Solver, Department of Mechanical Engineering, Standford University, USA, 1981–1987.
[5] E. Bazzo, Geração de vapor, segunda ed., Editora da UFSC, Florianópolis, Brasil, 1995, pp. 18–26.
[6] T.J. Kotas, The Exergetic Method of Thermal Plant Analysis, reprint ed. from the 1st ed., Krieger Publishing Company, Malabar, USA, 1995, pp. 236–262.
[7] S.A. Klein, F.L. Alvarado, Engineering Equation Solver: Professional, Version 6.596, F-Chart Software, Middleton, USA, 1992–2001.

**José Alexandre Matelli** is PhD student of the Mechanical Engineering Department of the Federal University of Santa Catarina and fellow researcher of the Laboratory of Combustion and Thermal System Engineering, being responsible for the researches in cogeneration and fuel cells.

**Edson Bazzo** is professor at the Mechanical Engineering Department of the Federal University of Santa Catarina and coordinator of several projects relate to power generation, cogeneration, clean energy applications and capillary pumping system, having published over 130 papers published at international conferences and journals related to these subjects plus a textbook related to steam generation.